IAC–24–C2.3.4

Actively Controlled Deployable Polymer Reflectors for Small Satellite Applications

Carl Johan G. Nielsen[a*], Michel Géradin[b], Julie Passion[c], Damien Robert[d], Thomas Godfroid[e], André Preumont[f]

[a] *Université Libre de Bruxelles, Belgium, carl.nielsen@ulb.be*
[b] *University of Liège, Belgium and TUM Institute for Advanced Study, Germany, mgeradin@gmail.com*
[c] *MateriaNova Mons, Belgium, julie.passion@materianova.be*
[d] *MateriaNova Mons, Belgium, damien.robert@materianova.be*
[e] *MateriaNova Mons, Belgium, thomas.godfroid@materianova.be*
[f] *Université Libre de Bruxelles, Belgium, andre.preumont@ulb.be*
[*] *Corresponding author*

Abstract

The presentation will report on the Advanced Multilayer Adaptive Thin Shell (AMATS) project aimed at developing actively controlled deployable primary reflectors with collecting area significantly larger than the size of the satellite. The project, supported by the ESA GSTP program, involves MateriaNova (Mons, Belgium) and Université Libre de Bruxelles (ULB). By utilizing a flexible polymer substrate material with an integrated piezoelectric polymer control layer, the reflector can be folded into a small space while using active control to compensate for thermal, viscoelastic and manufacturing errors.

The targeted applications are in the Long Wave Infrared (LWIR, $\lambda = 10$ μm) which is gaining interest for Earth observation, astronomical applications, and up- and downlink laser satellite communication (because data transmission under adverse weather conditions is possible in LWIR). These applications would benefit enormously from the increase of the reflector size while the surface figure accuracy for LWIR seems to be achievable with active control.

The project builds on a previous demonstration of the control of a spherical thin polymer shell using a piezoelectric polymer (PVDF-TrFE) activated by an array of independent electrodes on the back side of the reflector. In the AMATS project, the design has been improved by the addition of a thermal balancing layer, and the geometry is being adapted to a petal-design suitable for folding into a 3U CubeSat. The paper will report results on: 1. The development of an in-lab metrology system for the measurement of petal-shaped reflector samples. 2. The thermal response of thermally balanced coupon samples. 3. The estimation of piezoelectric coefficients from dynamic experiments before and after irradiation. 4. The numerical simulation of the folding-deployment phases and the estimation of the folding stresses.

Acronyms/Abbreviations
SCOTS: Software Configurable Optical Testing System
PVDF-TrFE: Poly(vinylidene fluoride-trifluoroethylene)
LWIR: Long Wave Infrared
PEI: Polyetherimide
PET: Polyethylene terephthalate

1. Introduction

The performance of imaging systems is governed strongly by the aperture diameter, because it influences both the light-gathering power as well as the attainable resolution. However, for small satellites the aperture is severely constrained. Deployable telescopes are one way to attain larger apertures and thus performance gains in small form factor satellites such as CubeSats. Although most conceptual designs feature rigidly deployable structures such as [1], [2], this paper concerns a foldable piezoelectric polymer actively controlled flexible reflector.

The reflector is a curved polymer substrate with integrated active control. The active control is attained by depositing patterned Aluminium electrodes, followed by a piezoelectric PVDF-TrFE layer, and finally an aluminium ground electrode. When a voltage is applied between the Aluminium layers, the piezoelectric material expands or contracts in the plane, causing a precise deformation of the mirror. The advantage of such a reflector is a simpler deployment mechanism, less mass, and highly integrated control. The concept is illustrated in Fig. 1. Further, Fig. 2 shows the deployment of a passive prototype. Four key issues will be addressed:

1. As shown in Fig.1, the reflector will be cut into segmented petals. This makes in-lab metrology more challenging, and a short review of methods devel-

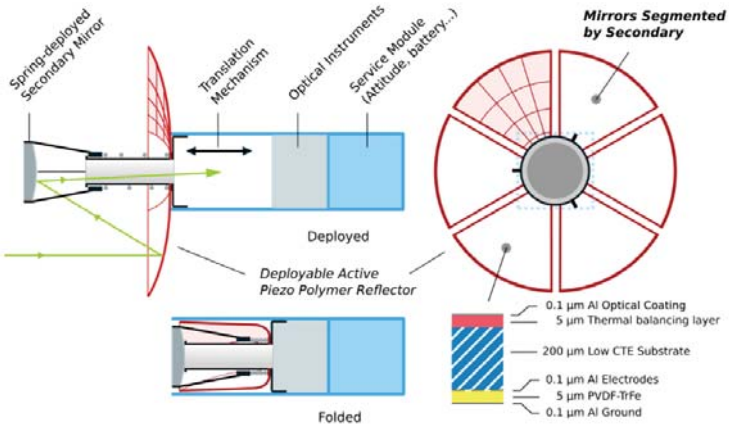

Fig. 1. System overview of the deployable reflector telescope. The PVDF-TrFE provides active control, allowing thermal and deployment aberrations to be controlled in orbit.

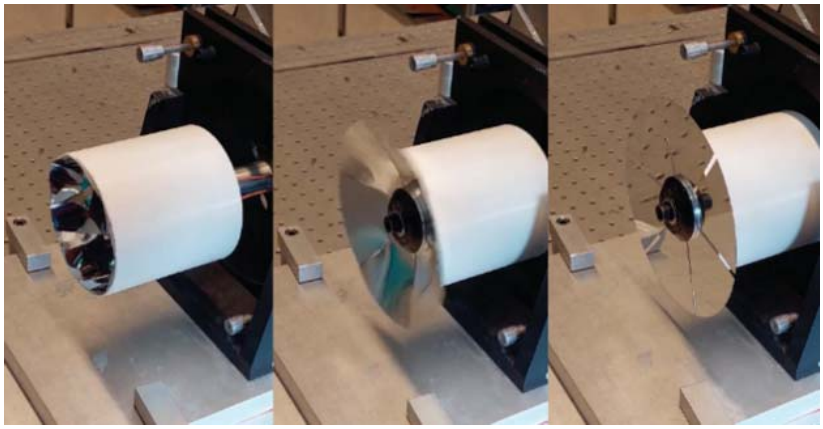

Fig. 2. Deployment stages of the polymer reflector. In the experimental setup, the reflector base is stationary while the cylinder moves, to facilitate metrology.

oped in the group to address this will be discussed. The in-lab metrology is based on the Software Configurable Optical Testing System (SCOTS) method, using phase unwrapping techniques suitable for complex domains.

2. The SCOTS method is further applied to the experimental characterization of the thermal performance of the reflector. The Coefficient of Thermal Expansion of the PVDF-TrFE is significantly higher than the polymer substrate. The reflector must therefore be thermally balanced. The balance is attained by dip-coating, which is a symmetric process. Small coupon samples are tested in balanced and unbalanced configurations.

3. When the reflector is in the space environment, it will be subjected to various types of radiation, and it must be demonstrated that piezoelectric performance can be maintained. For this reason, coupon samples with a single electrode have been tested before and after being subjected to 20 krad of x-ray and proton radiation. We observe no significant degradation of performance.

4. When the reflector is in its stowed state, the polymer substrate will undergo a relaxation process. Subsequent deployment of the reflector will thus be subject to an aberration while the material recovers. A numerical study has been conducted using a nonlinear shell model and viscoelastic material model. The shell geometry is folded, stored, deployed, and the expected aberration is investigated to determine the time required before the deployment aberration be-

comes within the control stroke of the PVDF-TrFE active control.

2. In-lab Metrology Using Modified SCOTS

The SCOTS method as envisioned in [3], [4], [5] is a variant of deflectometry, where a camera images the reflection of a known pattern on a test subject in order to determine the shape of the test subject. The test is illustrated in Fig.3.

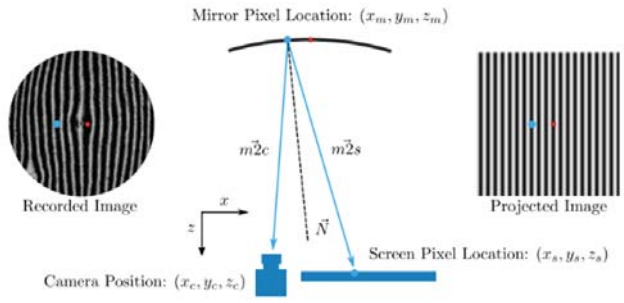

Fig. 3. Illustration of the SCOTS process. The red dot is the zero-phase location which is determined separately. Once the zero-phase location is known, the two vectors $\vec{m2c}$ and $\vec{m2s}$ can be determined by relating points on the recorded image with the projected image.

The known pattern is usually a sinusoidal fringe map which is displayed on a PC monitor, and the critical part of the SCOTS test is relating the phase map of the recorded image with the projected image, such that the location of any point on the reflector (Mirror Pixel Location) can be related to any point on the screen (Screen Pixel Location). The step is not trivial, because the phase in any individual point can only be known from $-\pi$ to π unless the whole phase map is considered. Once the relationship is known through phase unwrapping techniques, the vectors $\vec{m2c}$ and $\vec{m2s}$ in Fig.3 can be constructed, and from these the slope map of the reflector can be found (or the final shape, with integration).

To allow the measurement of complex geometries, a weighted phase unwrapping technique is used [6] using the petal geometry as a mask. The discontinuity-preserving Mumford-Shah integration technique is used to recover the shape from slope data [7].

Using raytracing, the metrology can be tested numerically. First, an aberrated reflector shape is generated by applying a tip displacement in a finite element shell model, leading to a realistic physical shape shown in Fig.4. Raytracing of a sinusoidal fringe map reflected in the 3D model leads to the image in Fig.5. By generating several images and using the phase unwrapping algorithm, slope calculation, and integration techniques, the shape of the reflector is recovered in Fig.6, and the error from the nominal result is shown in Fig.7.

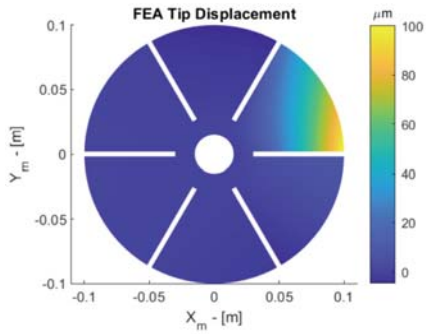

Fig. 4. Example aberration of the reflector in which a 100 micron tip displacement is applied.

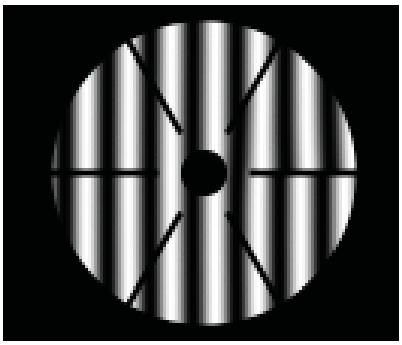

Fig. 5. Raytraced example image of reflected pattern. The aberration is apparent by the shifting of the fringes.

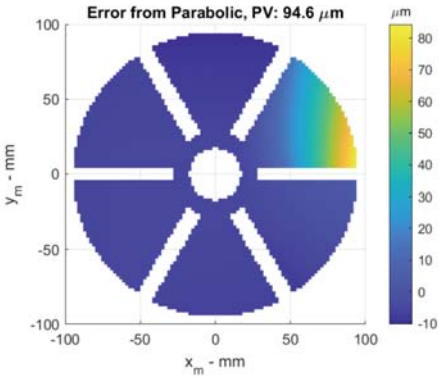

Fig. 6. Recovered error after phase unwrapping, slope determination, and integration.

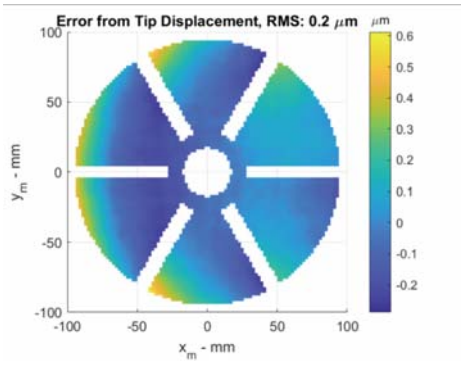

Fig. 7. Error between applied and measured displacement.

Further explanations as well as discussion on the assumptions which lead to the small discrepancy (submicron) are discussed in [8]. We note that, for the purposes of the polymer reflector study, the accuracy is sufficient and demonstrates the capability to measure the complex geometries in the lab. The test is central to the work and is being used to characterize manufacturing errors of the polymer substrate, thermal performance and viscoelastic behaviour during unfolding.

3. Thermal Balancing of Coupon Samples

Using the same measurement techniques as explained in the preceding section, the thermal stability is tested on three coupon samples in a vacuum chamber under radiative heating on the back side of the samples. The vacuum helps to maintain equal temperature on both sides of the samples, because heat is lost to the environment very slowly (thus, the applied heat is distributed easily in the samples). The concept is illustrated in Fig.9.

The samples are as follows:

1. The **top coupon** is PEI balanced with aluminium (Al) on both sides.
2. The **middle coupon** is unbalanced with Al on both sides and PVDF only on one side.
3. The **bottom coupon** is balanced with Al and PVDF on both sides.

All coupons have PEI as substrate, with thickness 175 μm. The thickness of the PVDF-TrFE layer is 5 μm. The thermal stability of the top and bottom samples (balanced) is good, whereas the middle sample (unbalanced) is poor.

By imposing the known boundary condition (clamped beam) on the left side of the samples, the shape is reconstructed, and the change in shape is found for all three beams.

The results are shown in Fig.8, which suggest a reduction in thermal deformation by a factor of seven for the balanced sample with PVDF on both sides versus the unbalanced sample. Under perfect conditions, we would expect no deflection in the balanced samples. The slight deflection of the balanced samples can be explained by temperature difference of the front and back side, or uneven application of balancing layers.

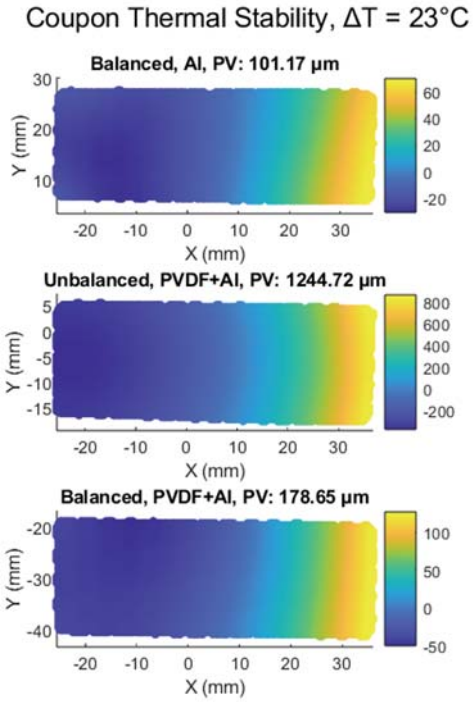

Fig. 8. Coupon thermal stability. The thermal deflection of the balanced sample is around seven times better than the unbalanced sample.

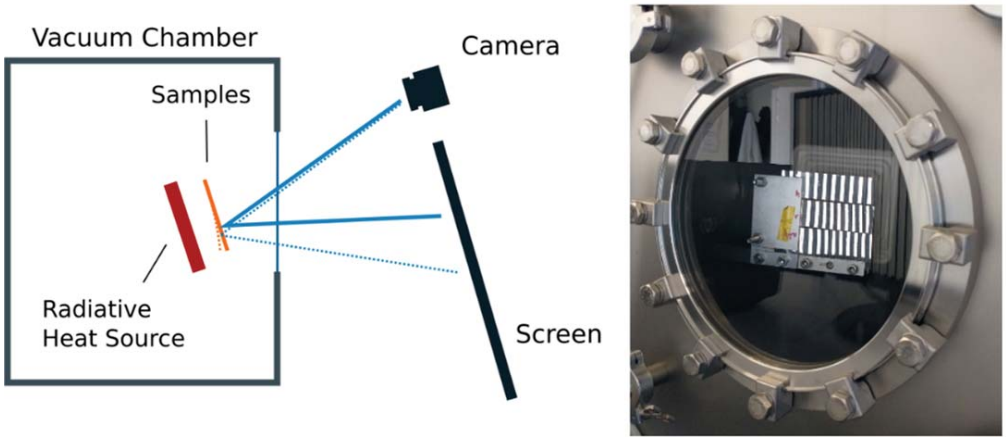

Fig. 9. Experimental setup for thermal stability test. When samples are heated uniformly by the radiative source in vacuum, the camera and screen setup can detect small changes in angle. The setup is angled to avoid reflections in the chamber viewport.

4. Active Control after Irradiation

To ensure that the piezoelectric polymer PVDF-TrFE can maintain adequate performance in the space environment, the piezoelectric coefficient d_{31} is tested before and after material samples are subject to irradiation. The material samples are made of PEI and have PVDF-TrFE and Aluminium electrodes on both the mirror and back sides. Two samples are shown in 10. Coupon C2 will be subjected to a proton radiation of 20 krad, C8 will be subjected to an X-ray radiation of 20 krad.

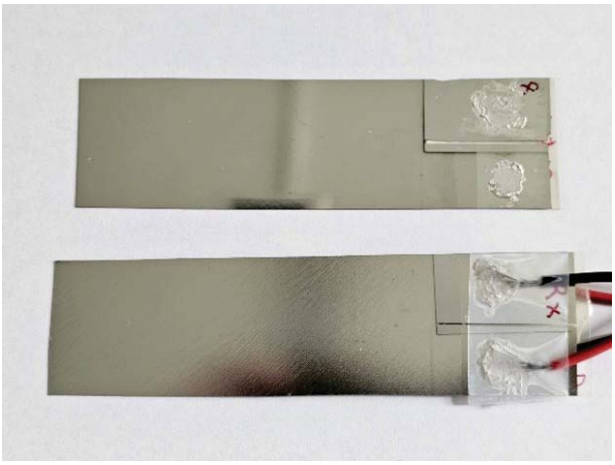

Fig. 10. PEI samples with PVDF-TrFE and electrodes on both sides. (top) Coupon 8, mirror side (bottom) Coupon 2, back side.

The coefficient can be determined using a dynamic testing method in which the frequency response of a clamped coupon subject to voltage-driven forced vibration is measured and compared to a numerical model of the system. In the experimental setup a dynamic signal analyser outputs a white noise signal, which is amplified and used to drive the coupon electrode. A fiber interferometer obtains the velocity response and the frequency response is finally computed. The experimental setup is shown in 11.

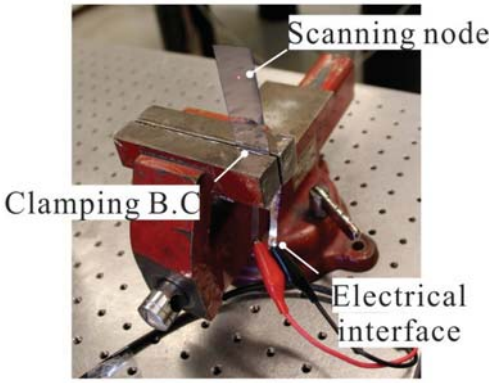

Fig. 11. Experimental setup showing the sample to be measured, along with the clamp and scanning node where the velocity response is obtained. Illustration: [9]

In the numerical model, a voltage-driven coupon is modelled and a state space model is described for the scanning node, allowing to compute the expected frequency response similar to the experiment. By comparing the frequency response of the experiment with the numerical simulation, the stiffness and d_{31} are varied to obtain a final result. The advantage of the test is that the equivalent stiffness of the sample is determined (by matching the natural

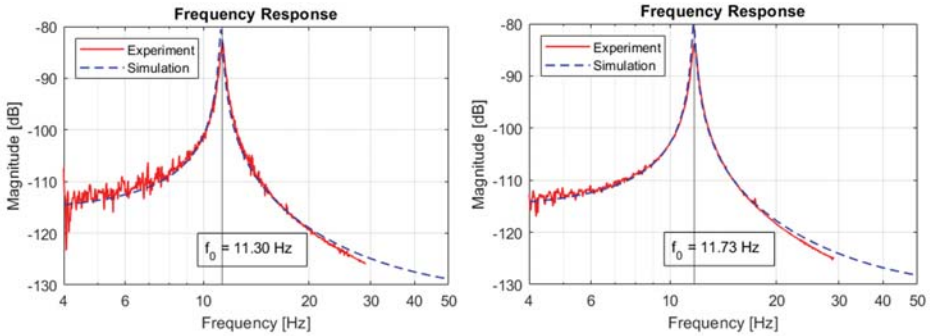

Fig. 12. Experimental and simulated frequency response function for the back-side of Coupon 2 before (left) and after (right) being subjected to 20 krad proton radiation.

frequency of experiment and simulation) at the same time as the piezoelectric performance. Conversely, a static test would require an accurate measurement of the stiffness of the beam, which may be difficult particularly if the sample is not completely flat. Further explanation of the test can be found in [10].

An example of the test is shown in Fig.12 for the back side of coupon 2 before and after irradiation. Two measurements at different sample lengths have been carried out, and the average piezoelectric coefficient is computed, and given in Table 1.

Table 1. Average piezoelectric coefficients of the samples before and after irradiation. (Mirror) refers to the mirror-side of the coupon sample.

	Coupon		
	2 (Mirror)	2 (Back)	8 (Mirror)
Before irradiation	12.25	15.0	11.5
After irradiation	11.25	16.75	10.5

The results can be adequately explained by experimental inaccuracies such as the exact height of the sample, scanning point, etc. Overall, we do not find a significant reduction in piezoelectric performance, and the results corroborate that of [11], in which PVDF is mentioned as being a particularly radiation resistant polymer.

5. Viscoelastic Simulation of Deployment Aberrations

In the stowed state, the polymer substrate material undergoes viscoelastic relaxation from its initial high stress state to a state of lower stress. The internal changes in the material are still present after deployment and lead to an aberration of the reflector in the unfolded state. The aberration is gradually reduced under viscoelastic recovery where the material recovers to its initial state. The process is reversible only up to a limit of stress, which for the materials considered is around a third of the yield strength [12]. Thus, the first step is to ensure that the material remains below this limit. Subsequently, a viscoelastic model can be implemented. In this section, both a numerical model of the problem and a preliminary experiment will be considered.

5.1 Viscoelastic Modelling of the Reflector

A nonlinear shell model is used for the problem. Fig. 13 shows an illustration of the numerical simulation, in which external boundary conditions are applied. The boundary conditions are reduced from a diameter of 20 cm to a diameter of 10 cm, folding the reflector within the allotted stowed space. Upon folding, the internal stress state can be found and is shown in Fig. 14.

The viscoelastic model used is the generalized Maxwell model (Prony series), which is illustrated in Fig. 15. The model consists of a spring which governs the long-term behaviour of the material, as in a linear elastic material. A series of Maxwell units governs the viscoelastic behaviour on differing timescales. To classify the material, it is necessary to test the properties on many different timescales. For the purpose of this study, we have used just two Maxwell units, for which experimental data is available in a relevant timescale [13]. Faster-acting Maxwell units are not included, because their contribution in a forced displacement problem can be neglected if only the long-term effects are of importance (the dashpot will quickly relax to a state of zero stress and then quickly recover after deployment).

Using material data from [13], the viscoelastic recovery of the reflector is demonstrated in Fig. 16. The influence of the temperature is also considered. Following

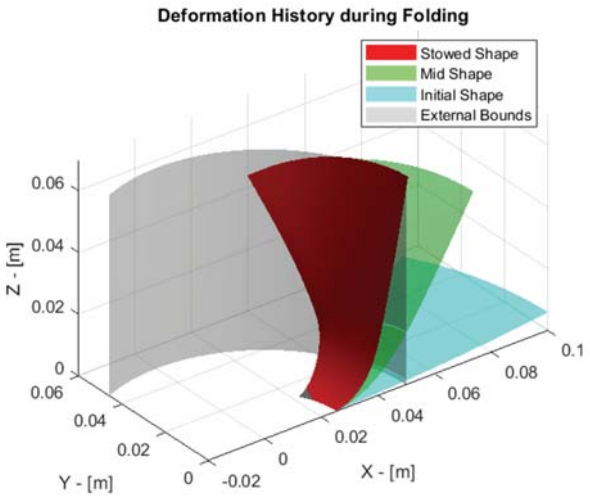

Fig. 13. Illustration of the folding stage during numerical simulation. The diameter of the external bounds is gradually reduced, causing the reflector to fold into the stowed state. Half a petal is shown.

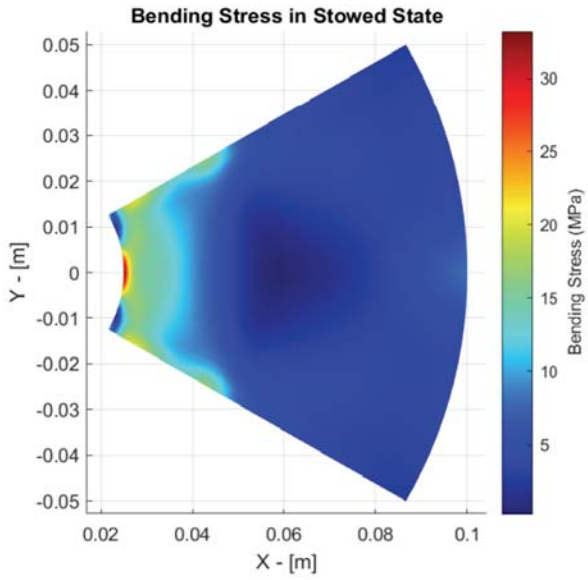

Fig. 14. Internal stress state (von Mises bending stress) in the reflector in its folded state. The maximum stress is less than one third of the yield strength, making the use of a reversible viscoelastic model reasonable.

the 24 hours storage, the aberration is relatively quickly recovered.

The numerical simulations were performed using a viscoelastic shell finite element and a contact algorithm

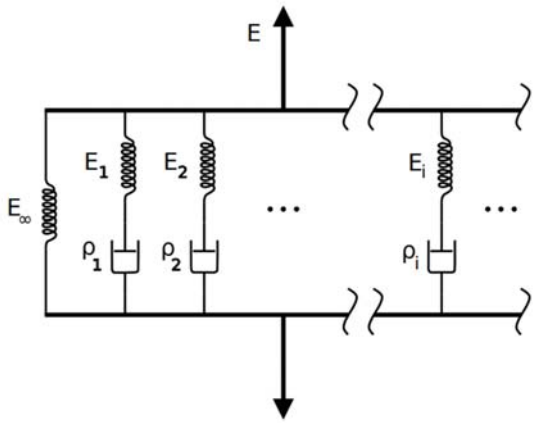

Fig. 15. Prony series viscoelastic model of the reflector.

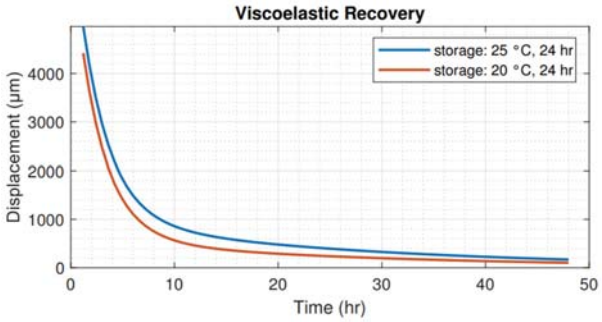

Fig. 16. Numerical viscoelastic recovery of the reflector after storage at two different temperatures for 24 hours. Two Maxwell units in material model.

specifically developed and implemented in the JuDyn software [14] in support of this project.

5.2 Viscoelastic Experiment

The deployment of the reflector was illustrated in Fig. 2, and the experimental setup shown is the basis for a storage and unfolding experiment. The reflector material is PET for this initial prototype, although we expect a change to PEI because of more isotropic properties. The metrology is based on the SCOTS metrology which was explained in Section 1, and illustrated in Fig. 3. The reflector is mounted on a permanent base, and a moving cylindrical housing is used to fold the reflector in the stowed configuration. This configuration makes metrology easier, because the reflector position must be the same to compare measurements before and after folding. Measurements are taken before storage as well as after storage, and the deviation of 6 points (one per petal) is tracked for 16 hours during the viscoelastic unfolding phase, shown in Fig. 17.

The 6 points are illustrated along with the final aberration for the whole reflector in Fig. 18. The temperature is also tracked in order to compensate for potential temperature drift (although this has so far been unnecessary). The results are preliminary, and only a storage period of 2 hours has been considered so far. Further study will look into longer storage as well as identification of viscoelastic parameters from the experimental data. The initial deformations are smaller than what is shown in the numerical experiment (Fig. 16), which is expected given the shorter storage time. We note that the initial error is outside the envelope of control of the reflector, while after 16 hours, the aberration is within the range of control. The final aberration of the reflector is not uniform, which is ascribed to the anisotropy of the PET material as well as the folding order, with petals 2 and 6 likely experiencing a slightly stronger bending in this initial prototype.

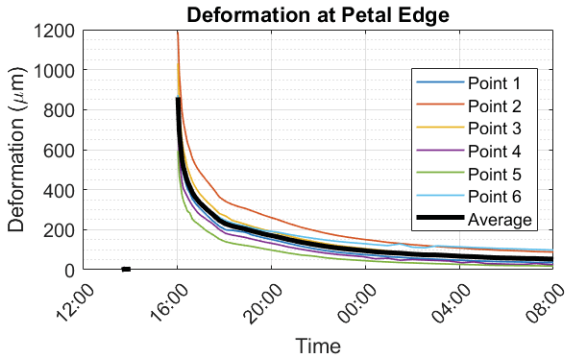

Fig. 17. Measured viscoelastic recovery over 16 hours of the reflector (Figure 2) after storage of 2 hours. The average as well as the individual deformations of the 6 petals are shown. The measured points are shown in Figure 18. The reversibility of the viscoelasticity is apparent.

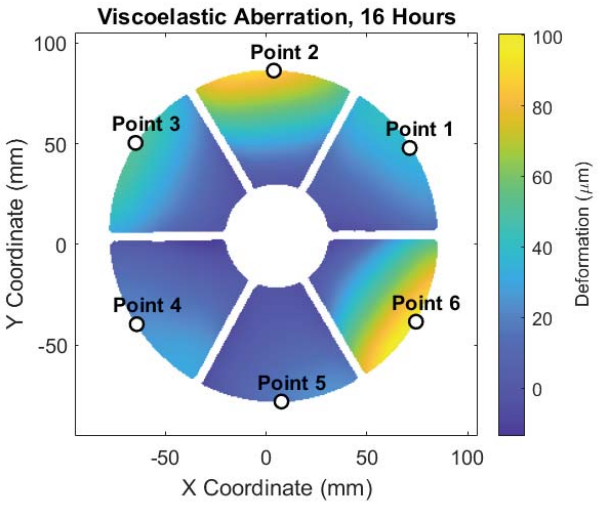

Fig. 18. Measured viscoelastic aberration 16 hours after unfolding from 2 hour storage. The difference in aberrations between the reflector petals is explained by the anisotropy of the PET material as well as the folding order.

5.3 Active Control of Residual Aberration

Finally, we consider the control envelope of the reflector, as the voltage applied to the material is limited. In Fig. 19, the influence functions of each individual electrode are calculated in FEM, and used to model the control of the reflector. A best-fit correction is found, and the residual error and electrode voltages are determined.

The example viscoelastic aberration used is the numerical result, 48 hours after the petal has been released from its 24 hour storage (Fig. 16). The electrode control voltages are well within the range of control, which for practical purposes is on the order of 300 V. For aberrations of this magnitude, the residual error is still outside the range of operation in the visible or LWIR wavelengths. However, it is well within the range of control with MEMS adaptive mirrors.

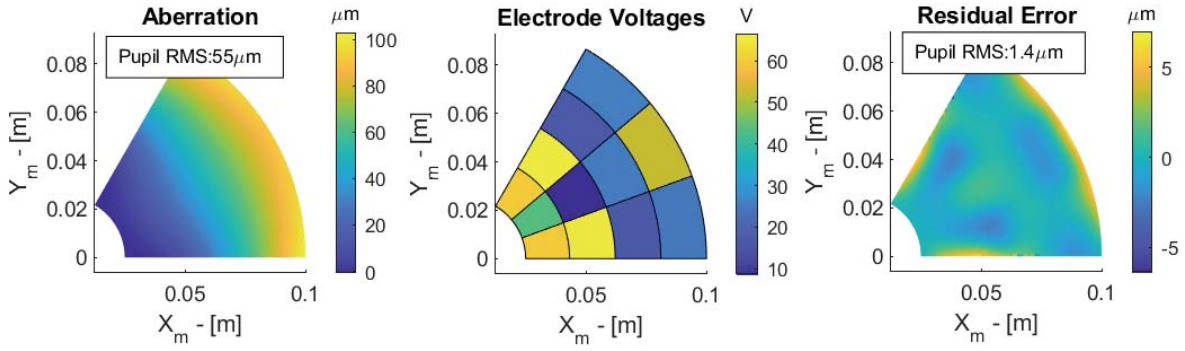

Fig. 19. Active control of the reflector from the viscoelastic deployment aberration. Control voltages are well within the range of control, and residual errors are within the range of MEMS adaptive optics.

6. Conclusion

The in-lab metrology, thermal stability, and viscoelastic deployment have been considered for the actively controlled piezoelectric polymer reflector. It was shown that metrology is feasible using a variation of the SCOTS test. Raytracing allows for a full numerical simulation of the metrology, and with assumptions explained in [8], a sufficiently low aberration is demonstrated.

The SCOTS test was also used to explore the thermal stability of coupon samples before scaling the dip-coating process to the full reflectors. A seven times reduction in the bending of samples was demonstrated with a balanced PVDF-TrFE layer as opposed to a single-sided configuration.

Finally, the numerical simulation of the folding indicated stresses less than a third of the substrate material's yield strength, indicating a reversible viscoelastic model is applicable. Simulation of stowage and deployment (relaxation and recovery) indicates a drop in aberration to 100 microns after two days, which is within the control envelope of the PVDF-TrFE. Likewise, a preliminary experimental result is reported on, but it is too early to draw conclusions here, since a different material is used and the storage period is short.

Acknowledgements

The authors acknowledge the support of the ESA GSTP program under the Advanced Multilayer Adaptive Thin Shells (AMATS) project.

References

[1] J. Champagne, S. Hansen, T. Newswander, and B. Crowther, "Cubesat image resolution capabilities with deployable optics and current imaging technology,"

[2] N. Schwartz *et al.*, "High-resolution deployable cubesat prototype," in *Space Telescopes and Instrumentation 2020: Optical, Infrared, and Millimeter Wave*, SPIE, vol. 11443, 2020, pp. 565–577.

[3] P. Su, R. Parks, L. Wang, R. Angel, and J. Burge, "Software configurable optical test system: A computerized reverse hartmann test," *Applied optics*, vol. 49, no. 23, pp. 4404–4412, 2010.

[4] J. Burge, P. Su, G. Butel, R. Huang, A. Maldonado, and T. Su, "Measuring large mirrors using scots: The software configurable optical test system," in *Advances in Optical and Mechanical Technologies for Telescopes and Instrumentation*, SPIE, vol. 9151, 2014, pp. 311–323.

[5] A. Lowman, G. Smith, L. Harrison, S. West, and C. Oh, "Measurement of large on-axis and off-axis mirrors using software configurable optical test system (scots)," in *Advances in Optical and Mechanical Technologies for Telescopes and Instrumentation III*, SPIE, vol. 10706, 2018, pp. 405–418.

[6] D. Ghiglia and L. Romero, "Robust two-dimensional weighted and unweighted phase unwrapping that uses fast transforms and iterative methods," *JOSA A*, vol. 11, no. 1, pp. 107–117, 1994.

[7] Y. Quéau, J.-D. Durou, and J.-F. Aujol, "Variational methods for normal integration," *arXiv preprint arXiv:1709.05965*, 2017.

[8] C. Nielsen and A. Preumont, "Adaptive petal reflector: In-lab software configurable optical testing system metrology and modal wavefront reconstruction," *Sensors*, vol. 23, no. 17, p. 7316, 2023.

[9] *Multilayer adaptive thin shell reflectors for future space telescopes (MATS), TN 4.3*.

[10] K. Wang, T. Godfroid, D. Robert, and A. Preumont, "Electrostrictive pvdf-trfe thin film actuators for the control of adaptive thin shell reflectors," *Actuators*, vol. 9, no. 3, 2020, ISSN: 2076-0825. DOI: 10.3390/act9030053. [Online]. Available: https://www.mdpi.com/2076-0825/9/3/53.

[11] G. Jones *et al.*, "Characterization, performance and optimization of PVDF as a piezoelectric film for advanced space mirror concepts.," SAND2005-6846, 876343, Nov. 1, 2005, SAND2005–6846, 876 343. DOI: 10.2172/876343. [Online]. Available: https://www.osti.gov/servlets/purl/876343/ (visited on 09/09/2024).

[12] J. Jansons, A. Aniskevich, and L. Pazhe, "Analysis of reversible and irreversible strains in the creep of a nonlinear viscoelastic polymer," *Mechanics of Composite Materials*, vol. 48, no. 2, pp. 209–216, 2012.

[13] A. Allen, A. Mashin, and K. Kwok, "Onset of creasing in polymer thin membranes," in *AIAA SCITECH 2022 Forum*, American Institute of Aeronautics and Astronautics, 2021.

[14] M. Géradin, *JuDyn: A julia package for flexible multibody dynamics*, Available at https://github.com/michelg45/JuDyn.jl, 2024.